Electronic Supplementary Information

Half-sandwich Ruthenium(II) Complexes Containing N^N-chelated Imino-pyridyl Ligands That Are Selectively Toxic to Cancer Cells

Meng Tian†, Juanjuan Li†, Shumiao Zhang, Lihua Guo, Xiangdong He, Deliang Kong, Hairong Zhang, Zhe Liu*

Institute of Anticancer Agents Development and Theranostic Application, The Key Laboratory of Life-Organic Analysis and Key Laboratory of Pharmaceutical Intermediates and Analysis of Natural Medicine, Department of Chemistry and Chemical Engineering, Qufu Normal University, Qufu 273165, China.

†The first two authors are equal first authors.

*Corresponding author. Email: liuzheqd@163.com

Abstract

Supporting information includes the experimental details and data. The experimental section includes the materials and instruments, the synthesis of the ligands (**L_1-L_4**) and complexes **1-4** [(η^6-bz)Ru(N^N)Cl]PF_6. Experimental data include the crystallographic data, hydrolysis chemistry, nucleobase binding, BSA interactions, cell toxicity, cellular uptake, catalytic hydride transfer analysis, cell cycle, ROS induction, apoptosis and mitochondrial membrane assay.

EXPERIMENTAL SCETION

Materials and Instrumentation.

All the synthesis operations were performed in a nitrogen atmosphere. $RuCl_3 \cdot nH_2O$, 2,6-dimethylaniline, 2,6-diisopropylaniline, 1-(pyridin-2-yl)ethanone, picolinaldehyde, quinoline-2-carbaldehyde, 9-ethylguanine, and 9-methyladenine were purchased from Sigma-Aldrich. For the biological experiments, BSA, DMEM medium, fetal bovine serum, penicillin/streptomycin mixture, trypsin/EDTA, cisplatin, MTT, and phosphate-buffered saline (PBS) were purchased from Sangon Biotech. Testing compounds was dissolved in DMSO and diluted with the tissue culture medium before use. Stock solutions of cisplatin (10 mM) and complexes **1–4** (10 mM) were prepared in DMSO. All stock solutions were stored at -20 °C, thawed and diluted with culture medium prior to each experiment.

X-ray Crystallography. All diffraction data were obtained on a Bruker Smart Apex CCD diffractometer equipped with graphite-monochro mated Mo Kα radiation. Absorption corrections were applied using SADABS program. The crystals were mounted in oil and held at 100 K with the Oxford Cryosystem Cobra. The structures were solved by direct methods using SHELXS (TREF) with additional light atoms found by Fourier methods. Complexes were refined against F^2 using SHELXL, and hydrogen atoms were added at calculated positions and refined riding on their parent atoms. X-ray crystallographic data for complex **2** are available as Fig. **1**, Tables **S1** and **S2** have been deposited in the Cambridge Crystallographic Data Centre under the accession numbers CCDC 1567186. X-ray crystallographic data in CIF format are available from the Cambridge Crystallographic Data Centre (http://www.ccdc.cam.ac.uk/).

NMR Spectroscopy. ^{1}H NMR spectra were acquired in 5 mm NMR tubes at 298 K on Bruker DPX 500 (^{1}H = 500.13 MHz) spectrometers. ^{1}H NMR chemical shifts were internally referenced to $(CHD_2)(CD_3)SO$ (2.50 ppm) for DMSO-d_6, $CHCl_3$ (7.26 ppm) for chloroform-d_1. All data processing was carried out using XWIN-NMR version 3.6 (Bruker UK Ltd.).

UV-Vis Spectroscopy. The UV-Vis spectra of the compounds were recorded by TU-1901 UV spectrophotometer with 1 cm path-length quartz cuvettes (3 ml). Spectra were processed using UVWinlab software. Experiments were carried out at 298 K unless otherwise stated.

Hydrolysis Studies. Solutions of complex **4** with final concentrations of 1 mM in 50% CD_3OD /50% D_2O (v/v) were prepared by dissolution of the complex in CD_3OD followed by rapid dilution with D_2O. ^{1}H NMR spectra were recorded after various time intervals at 310 K. Solutions of complex **4** with final concentrations of 50 μM in 30% MeOH/70% H_2O (v/v) were prepared by dissolution of the complex in MeOH followed by rapid dilution with H_2O. UV-Vis spectra of these solutions were recorded at 298 K after various time intervals.

Interaction with Nucleobases. The reaction of complex **4** (ca. 1 mM) with nucleobases typically involved addition of a solution containing 1 mol equiv of nucleobase in D_2O to an solution of complex **4** in 50% CD_3OD/50% D_2O (v/v). ^{1}H NMR spectra of these solutions were recorded at 310 K after various time intervals.

Reaction with NADH. The reaction of complexes **2** and **4** (ca. 1 μM) with NADH (ca. 100 μM) in 10% MeOH/90% H_2O (v/v) was monitored by UV-Vis at 298 K after various time intervals. TON was calculated from the difference in NADH concentration after 8 h divided by the concentration of ruthenium catalyst. The concentration of NADH was obtained using the extinction coefficient $\varepsilon_{339} = 6220\ M^{-1}cm^{-1}$.

Binding with BSA. The titration experiments including UV–Vis absorption and fluorescence quenching were performed at constant concentration of BSA. A BSA stock solution was prepared in Tris buffer (5 mM Tris–HCl/10 mM NaCl at pH 7.2) and stored at 4 °C. All spectra were recorded after each successive addition of the compounds and incubation at room temperature for 5 min to complete the interaction. The ruthenium complex was added to both sample cuvette and the reference cuvette in order to offset the self-absorption of iridium complex in the UV region. The fluorescence emission spectra of BSA in the absence and presence of Ru complex were recorded with excitation at 285 nm. The concentrations of the Ru complex were 0–10 μM, and the concentration of BSA was fixed at 10 μM. Synchronous fluorescence spectra of BSA with various concentrations of complexes (0–10 μM) were obtained from 240 to 500 nm when $\Delta\lambda$=60 nm and $\Delta\lambda$=15 nm.

In the UV–Vis absorption titration experiment, a BSA solution (2.5 ml, 10 μM) was titrated by successive additions of the stock solutions of Ru complex ($1x10^{-3}$ M) and the changes in the BSA absorption. After 10 min equilibration at room temperature, the absorption spectrum of BSA was recorded for each successive addition of the complex.

The UV-Vis absorption spectra of BSA in the presence of complex **4** are shown in Fig. **2A**. Complex **4** was added to both the sample cuvette and the reference cuvette in order to offset the self-absorption of **4** in the UV region. After the addition of **4** the absorption peak at 228 nm decreased significantly, which is due to interference to the α-helix of BSA by complex **4**.[1-3] With the addition of complex **4** to BSA, a progressive decrease without any shift was observed in the absorption peak of BSA at 278 nm, suggesting that the Ru complex interacted with the BSA molecule and the microenvironment of the three aromatic acid residues in BSA (Trp, Tyr and Phe) was altered.[4] Through the study of fluorescence quenching the binding capacity of **4** with BSA was further studied. The fluorescence measured in this work was calibrated to correct the ''inner filter'' effect.[5] The fluorescence emission spectra of BSA in the presence of complex **4** at various concentrations at 298 K are shown in Fig. **2B**. With an increase in the concentration of complex **4**, the fluorescence intensity of BSA gradually decreased, suggesting that complex **4** can interact with BSA *via* a static quenching mode. The possible quenching mechanism can be interpreted using the Stern–Volmer equation (eqn (1)):[6]

$$F_0/F = 1 + K_{sv}[Q] = 1 + K_q\tau_0[Q] \qquad (1)$$

where F_0 and F are the fluorescence intensities in the absence and presence of the quenching agent Q, [Q] represents the concentration of the quenching agent, K_q is the quenching rate constant and τ_0 is the average life expectancy of the fluorescent substance when the quencher does not exist, approximately 10^{-8} s.[7] K_{SV} is the Stern–Volmer constant which can be obtained from the ratio of the slope to the intercept of the plot of F_0/F *versus* the concentration of the tested complex (Fig. **S8,** ESI†). The results are listed in Table **S4**, ESI†. The calculated value of K_q for the complex is 4.77×10^{12} M^{-1} s^{-1}, which is about two orders of magnitude higher than that of the purely dynamic quenching mechanism (2.0×10^{10} M^{-1} s^{-1}).[8] Thus, this value of K_q indicates that a static quenching mechanism dominates in the interaction between the Ru complex and BSA. The binding constant K_b and the number of complexes bound to BSA (n) are calculated (Fig. **S9,** ESI†) using the following formula (eqn (2)):[9]

$$\log[(F_0-F)/F] = \log K_b + n \log[Q] \qquad (2)$$

The magnitudes of K_b and K_q of complex **4** are 10^4 M^{-1} and 10^{12} M^{-1} s^{-1}, respectively, indicating a medium binding ability to BSA.

Synchronous fluorescence spectrometry is a very useful technique for obtaining information about the molecular environment near fluorescence molecules. When the wavelength interval is stable at 15 nm or 60 nm, the synchronized fluorescence gives the characteristic information of tyrosine residues or tryptophan residues in BSA, respectively.[10] Fig. **S10** and **S11** (ESI†) show that the synchronous fluorescence intensity decreased gradually with the increase of concentration of complex **4** and red shifts of the wavelength of emission were observed, from 288 to 290 nm at $\Delta\lambda$ = 15 nm and from 280 to 289 nm at $\Delta\lambda$ = 60 nm, indicating that tyrosine was less involved than tryptophan in the combination of BSA and complex **4**.

Notes and References

1. R. Esteghamat-Panah, H. Hadadzadeh, H. Farrokhpour, M. Mortazavi and Z. Amirghofran, *Inorg. Chim. Acta*, 2016, **454**, 184-196.
2. J. Ruiz, C. Vicente, C. D. Haro and D. Bautista, *Inorg. Chem.*, 2013, **52**, 974-982.
3. F. Samari, B. Hemmateenejad, M. Shamsipur, M. Rashidi and H. Samouei, *Inorg. Chem.*, 2012, **51**, 3454-3464.
4. S. Tabassum, R. Singh, M. Zaki, M. Ahmad and M. Afzal, *Rsc Adv.*, 2015, **5**, 35843-35851.

5. M. E. Pacheco and L. Bruzzone, *J. Lumin.*, 2013, **137**, 138-142.
6. A. Castiñeiras, N. Fernández-Hermida, I. García-Santos and L. Gómez-Rodríguez, *Dalton Trans.*, 2012, **41**, 13486-13495.
7. R. Pettinari, F. Marchetti, A. Petrini, C. Pettinari, G. Lupidi, B. Fernández, A. R. Diéguez, G. Santoni and M. Nabissi, *Inorg. Chim. Acta*, 2017, **454**, 139-148.
8. J. Tang, F. Luan and X. Chen, *Biorg. Med. Chem.*, 2006, **14**, 3210-3217.
9. Z. Cheng, *J. Lumin.*, 2012, **132**, 2719-2729.
10. Y.-Z. Zhang, B. Zhou, Y.-X. Liu, C.-X. Zhou, X.-L. Ding and Y. Liu, *J. Fluoresc.*, 2008, **18**, 109-118.

Cell Culture. Both human cancer cells (cervical carcinoma HeLa cells and lung cancer A549 cells) and normal cells (human bronchial epithelial cells 16HBE and BESA-2B) were obtained from Shanghai Institute of Biochemistry and Cell Biology (SIBCB) and were grown in Dubelco's Modified Eagle Medium (DMEM). All media were supplemented with 10% fetal bovine serum, and 1 % penicillin-streptomycin solution. All cells were grown at 310 K in a humidified incubator under a 5 % CO_2 atmosphere.

Cellular uptake studies. A549 cells and BEAS-2B cells were seeded in 35 mm dishes for 24 h. The media was removed and replaced with fresh media containing the tested complexes (5 μM) for 24 h. After the removal of the culture media and rinse with 1 mL of PBS buffer (1X), the cells were treated with 500 μl of 0.25% trypsin and centrifuged at 1000 rpm. The cells were counted, and digested with concentrated nitric acid (65%, 225 μl) at 80 °C overnight. The solution was then diluted to a final volume of 3 ml with Milli-Q water. The concentration of ruthenium was determined directly by the inductively coupled plasma mass spectrometer (ICP-MS; VG Elemental). The experiment was performed in triplicate, and the average of the data was obtained.

Viability assay (MTT assay). After plating 5000 cells per well in 96-well plates, the cells were preincubated in drug-free media at 310 K for 24 h before adding different concentrations of the compounds to be tested. In order to prepare the stock solution of the drug, the solid complex was dissolved in DMSO. This stock was further diluted using cell culture medium until working concentrations were achieved. The drug exposure period was 24 h. Subsequently, 15 μl of 5 mg ml^{-1} MTT solution was added to form a purple formazan. Afterwards, 100 μl of dimethyl sulfoxide (DMSO) was transferred into each well to dissolve the purple formazan, and results were measured using a microplate reader (DNM-9606, Perlong Medical, Beijing, China) at an absorbance of 570 nm. Each well was triplicated and each experiment repeated at least three times. IC_{50} values quoted are mean ± SEM.

Cell Cycle Analysis. The A549 cancer cells at 1.5×10^6 per well were seeded in a six-well plate. Cells were preincubated in drug-free media at 310 K for 24 h, after which complexes **2** and **4** was added at concentrations of $0.25 \times IC_{50}$, $0.5 \times IC_{50}$, $1 \times IC_{50}$ and $2 \times IC_{50}$ of complexes **2** and **4** against A549 cancer cells. After 24 h of drug exposure, supernatants were removed by suction and cells were washed with PBS. Finally, cells were harvested using trypsin-EDTA and fixed for 24 h using cold 70 % ethanol. DNA staining was achieved by resuspending the cell pellets in PBS containing propidium iodide (PI) and RNAse. Cell pellets were washed and resuspended in PBS before being analyzed in a flow cytometer (ACEA NovoCyte, Hangzhou, China) using excitation of DNA-bound PI at 488 nm, with emission at 585 nm. Data were processed using NovoExpress™ software. The cell cycle distribution is shown as the percentage of cells containing G_0/G_1, S and G_2/M DNA as identified by propidium iodide staining. The cell cycle analysis was further performed for complex **4** in BEAS-2B normal cells using the same condition.

Induction of Apoptosis. Flow cytometry analysis of apoptotic populations of the cells caused by exposure to iridium complexes was carried out using the Annexin V-FITC Apoptosis Detection Kit (Beyotime Institute of Biotechnology, China) according to the supplier's instructions. Briefly, A549 cancer cells (1.5×10^6 /2 ml per

well) were seeded in a six-well plate. Cells were preincubated in drug-free media at 310 K for 24 h, after which complexes **2** and **4** was added at concentrations of 1 × IC_{50} and 3 × IC_{50} of complexes **2** and **4** against A549 cancer cells. After 24 h of drug exposure, cells were collected, washed once with PBS, and resuspended in 195 µl of annexin V-FITC binding buffer which was then added to 5 µl of annexin V-FITC and 10 µl of PI, and then incubated at room temperature in the dark for 15 min. Subsequently, the buffer placed in an ice bath in the dark. The samples were analyzed by a flow cytometer (ACEA NovoCyte, Hangzhou, China). The apoptosis analysis was further performed for complex **4** in BEAS-2B normal cells using the same condition.

ROS Determination. Flow cytometry analysis of ROS generation in the cells caused by exposure to iridium complexes was carried out using the Reactive Oxygen Species Assay Kit (Beyotime Institute of Biotechnology, Shanghai, China) according to the supplier's instructions. Briefly, 1.5 × 10^6 A549 cancer cells per well were seeded in a six-well plate. Cells were preincubated in drug-free media at 310 K for 24 h in a 5 % CO_2 humidified atmosphere, and then complexes **2** and **4** was added at concentrations of 0.25 × IC_{50} of complexes **2** and **4** against A549 cancer cells. After 24 h of drug exposure, cells were washed twice with PBS and then incubated with the DCFH-DA probe (10 µM) at 37 °C for 30 min, and then washed triple immediately with PBS. The fluorescence intensity was analyzed by flow cytometry (ACEA NovoCyte, Hangzhou, China). Data were processed using NovoExpress™ software. At all times, samples were kept under dark conditions to avoid light-induced ROS production. The ROS analysis was further performed for complex **4** in BEAS-2B normal cells using the same condition.

Mitochondrial Membrane Assay. Analysis of the changes of mitochondrial potential in cells after exposure to iridium complexes was carried out using the Mitochondrial membrane potential assay kit with JC-1 (Beyotime Institute of Biotechnology, Shanghai, China) according to the manufacturer's instructions. Briefly, 1.5 × 10^6 A549 cancer cells were seeded in six-well plates left to incubate for 24 h in drug-free medium at 310 K in a humidified atmosphere. Drug solutions, at concentrations of 0.25 × IC_{50} and 0.5 × IC_{50} of complexes **2** and **4** against A549 cancer cells, were added in triplicate, and the cells were left to incubate for a further 24 h under similar conditions. Supernatants were removed by suction, and each well was washed with PBS before detaching the cells using trypsin-EDTA. Staining of the samples was done in flow cytometry tubes protected from light, incubating for 30 min at ambient temperature. The samples were immediately analyzed by a flow cytometer (ACEA NovoCyte, Hangzhou, China). For positive controls, the cells were exposed to carbonyl cyanide 3-chlorophenylhydrazone, CCCP (5 µM), for 20 min. Data were processed using NovoExpress™ software. The mitochondrial membrane analysis was further performed for complex **4** in BEAS-2B normal cells using the same condition.

Syntheses.

Synthesis of the ligands (L_1-L_4).

General method: A solution of aldehyde or its derivative (20 mmol), arylamine (20 mmol), and a catalytic amount of formic acid in methanol (15 ml) was stirred at room temperature for 10 h. The solvent was evaporated to dryness on a rotary evaporator and a crude product was obtained, which was washed with water (5 ml) and dried over anhydrous at room temperature. The products were obtained as a white or yellow powder. The ^{1}H NMR (500.13 MHz, DMSO) peak integrals of **L_1**- **L_4** are shown in Figures **S21**-**S24**.

2,6-dimethyl-N-(pyridin-2-ylmethylene)aniline (**L_1**). Yield: 3.866 g, 92%. ^{1}H NMR (500 MHz, DMSO) δ 8.73 (ddd, J = 4.8, 1.6, 0.9 Hz, 1H), 8.30 (s, 1H), 8.23 (dt, J = 7.9, 0.9 Hz, 1H), 8.00 (ddd, J = 7.6, 1.7, 0.8 Hz, 1H), 7.58 (ddd, J = 7.5, 4.8, 1.2 Hz, 1H), 7.09 (d, J = 7.6 Hz, 2H), 6.99 – 6.94 (m, 1H), 2.08 (d, J = 8.0 Hz, 6H).

2,6-diisopropyl-N-(pyridin-2-ylmethylene)aniline (**L_2**). Yield: 5.057 g, 94%. ^{1}H NMR (500 MHz, DMSO) δ 8.77 – 8.69 (m, 1H), 8.26 (s, 1H), 8.21 (d, J = 7.8 Hz, 1H), 8.00 (s, 1H), 7.62 – 7.55 (m, 1H), 7.20 – 7.14 (m, 2H), 7.10 (dd, J = 8.5, 6.8 Hz, 1H), 2.86 (dt, J = 13.7, 6.9 Hz, 2H), 1.11 (d, J = 6.9 Hz, 12H).

2,6-diisopropyl-N-(1-(pyridin-2-yl)ethylidene)aniline (**L_3**). Yield: 5.267 g, 94%. ^{1}H NMR (500 MHz, DMSO) δ 8.72 – 8.68 (m, 1H), 8.26 (d, J = 7.9 Hz, 1H), 7.97 (td, J = 7.7, 1.8 Hz, 1H), 7.59 – 7.54(m, 1H), 7.16 (d, J = 7.7 Hz, 2H), 7.09 – 7.04 (m, 1H), 2.65 (dt, J = 13.7, 6.8 Hz, 2H), 2.12 (s, 3H), 1.11 (s, 3H), 1.10 (s, 3H), 1.08 (s, 3H), 1.07 (s, 3H).

2,6-diisopropyl-N-(quinolin-2-ylmethylene)aniline (**L_4**). Yield: 6.012 g, 95%. ^{1}H NMR (500 MHz, DMSO) δ 8.57 (d, J = 8.6 Hz, 1H), 8.43 (s, 1H), 8.36 (d, J = 8.5 Hz, 1H), 8.16 (d, J = 8.6 Hz, 1H), 8.11 (d, J = 7.4 Hz, 1H), 7.91 – 7.83 (m, 1H), 7.76 – 7.71 (m, 1H), 7.20 (d, J = 7.2 Hz, 2H), 7.17 – 7.10 (m, 1H), 2.92 (dt, J = 13.7, 6.9 Hz, 2H), 1.14 (d, J = 6.9 Hz, 12H).

Synthesis of the [(η^6-bz)Ru(N^N)Cl]PF_6.

General method: The corresponding Imino-quinolyl schiff base ligand **L_1-L_4** (0.10 mmol) and [(η^6-bz)$RuCl_2$]$_2$ (0.05 mmol) was dissolved in methanol (20 ml) in a dry round-bottom flask equipped with stirrer and nitrogen atmosphere. NH_4PF_6 (0.2 mmol) was added at room temperature with constant stirring for 4 h. The reaction mixture was stirred at room temperature for 20 h, and the progress of reaction was monitored by TLC. After complete conversion, methanol was removed under reduced pressure and product was dissolved in dichloromethane and filtered through Celite filtration funnel and recrystallized by slow diffusion of n-hexane in a concentrated solution of the compound in dichloromethane to obtain the corresponding complexes **1**−**4**. The ^{1}H NMR (500.13 MHz, DMSO) peak integrals of complexes **1-4** are shown in Figures **S25-S28**.

[(η^6-bz)Ru(L_1)Cl]PF_6 (**1**). Yield: 52%. ^{1}H NMR (500 MHz, DMSO-d_6) δ 9.69 (d, J = 5.4 Hz, 1H), 8.89 (d, J = 6.8 Hz, 1H), 8.32 (t, J = 8.4 Hz, 1H), 8.21 (d, J = 7.7 Hz, 1H), 8.00 – 7.87 (m, 1H), 7.46 – 7.14 (m, 3H), 5.88 (s, 6H), 2.38 (s, 3H), 2.18 (s, 3H). Anal. Calcd. For [(η^6-bz)Ru(L_1)Cl]PF_6 (569.87): C, 43.12; H, 3.96; N, 4.79. Found: C, 43.10; H, 4.02; N, 4.81. MS: m/z 425.25 [(η^6-bz) Ru(L_1)Cl]$^+$.

[(η^6-bz)Ru(L_2)Cl]PF_6 (**2**). Yield: 55%. ^{1}H NMR (500 MHz, DMSO-d_6) δ 9.73 (d, J = 5.3 Hz, 1H), 9.01 (s, 1H), 8.34 (td, J = 7.7, 1.3 Hz, 1H), 8.30 – 8.25 (m, 1H), 7.95 (ddd, J = 7.4, 5.6, 1.6 Hz, 1H), 7.55 – 7.38 (m, 3H), 5.89 (s, 6H), 3.71 (dt, J = 13.5, 6.7 Hz, 1H), 1.39 (t, J = 5.1 Hz, 1H), 1.30 – 1.21 (m, 6H), 1.12 (d, J = 6.7 Hz, 3H), 0.93 (d, J = 6.8 Hz, 3H). Anal. Calcd. For [(η^6-bz)Ru(L_2)Cl]PF_6 (625.98): C, 46.84; H, 4.87; N, 4.37. Found: C, 46.88; H, 4.33; N, 4.34. MS: m/z 563.25 [(η^6-bz)Ru(L_2)Cl+ CH_3COONa]$^+$.

[(η^6-bz)Ru(L_3)Cl]PF_6 (**3**). Yield: 50%. ^{1}H NMR (500 MHz, DMSO-d_6) δ 9.78 (d, J = 5.5 Hz, 1H), 8.41 – 8.25 (m, 2H), 7.98 – 7.88 (m, 1H), 7.57 – 7.44 (m, 3H), 5.86 (s, 6H), 1.41 (d, J = 6.7 Hz, 3H), 1.23 (d, J = 6.6 Hz, 3H), 1.01 (dd, J = 14.3, 6.8 Hz, 6H). Anal. Calcd. For [(η^6-bz)Ru (L_3)Cl]PF_6 (640.01): C, 47.67; H, 5.08; N, 4.28. Found: C, 47.62; H, 5.11; N, 4.31. MS: m/z 495.33 [(η^6-bz)Ru(L_3)Cl]$^+$.

[(η^6-bz)Ru(L_4)Cl]PF_6 (**4**). Yield: 60%. ^{1}H NMR (500 MHz, DMSO-d_6) δ 9.26 (s, 1H), 8.98 (d, J = 8.2 Hz, 1H), 8.79 (d, J = 8.9 Hz, 1H), 8.35 (t, J = 7.9 Hz, 2H), 8.24 (ddd, J = 8.7, 6.9, 1.5 Hz, 1H), 8.07 (dd, J = 11.2, 4.0 Hz, 1H), 7.59 – 7.55 (m, 2H), 7.50 (dd, J = 6.9, 2.2 Hz, 1H), 6.05 (s, 6H), 3.81 (dd, J = 13.6, 6.8 Hz, 1H), 2.64 (t, J = 6.7 Hz, 1H), 1.39 (d, J = 6.7 Hz, 3H), 1.32 (d, J = 6.7 Hz, 3H), 1.25 (d, J = 6.7 Hz, 3H), 0.91 (d, J = 6.8 Hz, 3H). Anal. Calcd. For [(η^6-bz)Ru (L_4)Cl]PF_6 (676.04): C, 50.40; H, 4.81; N, 5.13. Found: C, 50.37; H, 4.85; N, 5.16. MS: m/z 531.33 [(η^6-bz)Ru(L_4)Cl]$^+$.

Table S1. Crystallographic Data for [(η^6-bz)Ru(L_2)Cl]PF_6 (**2**).

	Complex **2**
formula	$C_{24}H_{28}ClF_6N_2PRu$

MW	625.97
Cryst size(mm)	0.42 × 0.40 × 0.34
λ (Å)	0.71073
temp(K)	295
cryst syst	Monoclinic
space group	P21/n
a (Å)	16.4797(11)
b (Å)	9.7608(6)
c (Å)	17.6390 (12)
α (°)	90
β (°)	115.5210(10)
γ (°)	90
vol($Å^3$)	2560.5(3)
Z	4
$R1_{[I>2sigma(I)]}$	0.0398
$wR2_{[I>2sigma(I)]}$	0.0983
GOF	1.046

Table S2. Selected Bond Lengths (Å) and Angles (deg) for [(η^6-bz)Ru(L_2)Cl]PF_6 (**2**).

	Complex **2**

Ru−C (phenyl)	2.172(4) 2.183(4) 2.186(4) 2.191(4) 2.197(4) 2.199(4)
Ru−C(centroid)	1.684
Ru−N_1	2.092(3)
Ru−N_2	2.092(3)
Ru −Cl	2.3928(9)
N_2− Ru−N_1	76.76(10)
N_1− Ru−Cl	81.93(8)
N_2− Ru−Cl	90.41(8)

Table S3. Hydrolysis Data for Complex **4** Monitored by UV-Vis at 298K.

Complex	k (min^{-1})	$t_{1/2}$ (min)
4	0.0052	134.6

Table S4. Quenching parameters and binding parameters for the interaction of the complex **4** with BSA.

Complex	T (K)	K_{sv} (10^4 M^{-1})	K_q (10^{12} $M^{-1}s^{-1}$)	K_b (M^{-1})	n
4	**298**	**4.77±0.18**	**4.77**	**1.86×104**	**1.628**

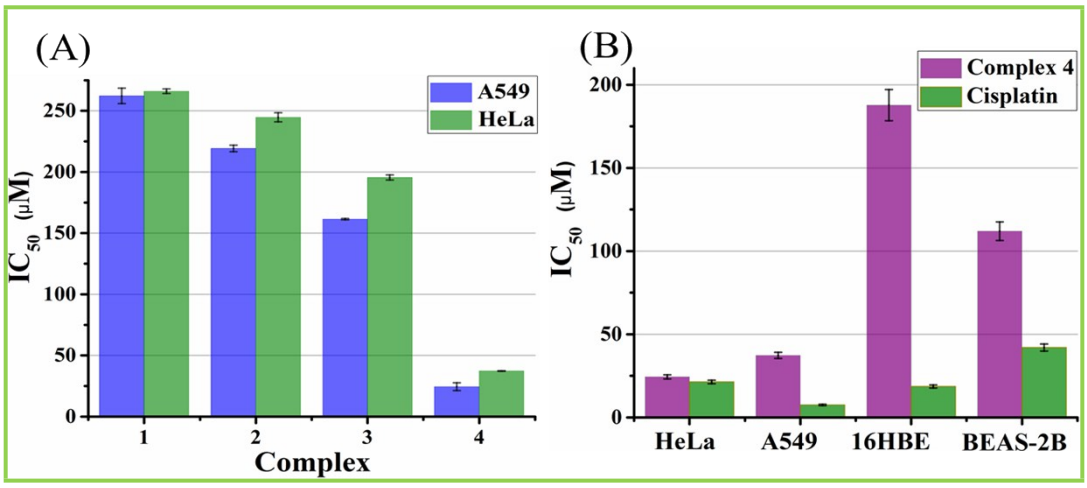

Figure S1. (**A**) IC_{50} values towards both A549 and HeLa cancer cells decreased with the order of complexes **1** > **2** > **3** > **4**. (**B**) Selectivity comparison between complex **4** and cisplatin against cancer cells and normal cells

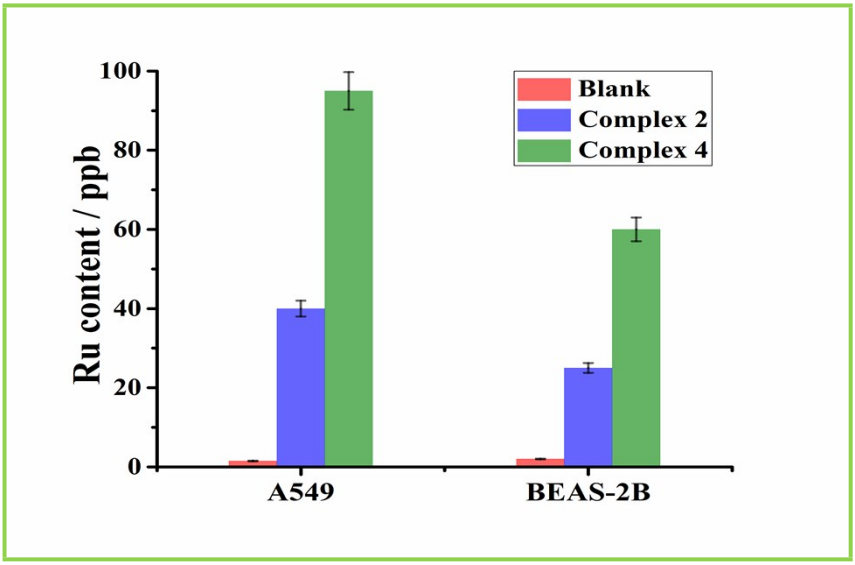

Figure S2. Ru content in 1 × 10^5 cells determined by ICP-MS measurement for the digestion solutions of A549 lung cancer cells and BEAS-2B human bronchial epithelial cells incubated, respectively, with complex **2** (5 μM) and complex **4** (5 μM). The incubated cells were digested for ICP-MS determination using a standard procedure after 24 h of incubation. Blank, Ru contents for the cells without any Ru complex incubation.

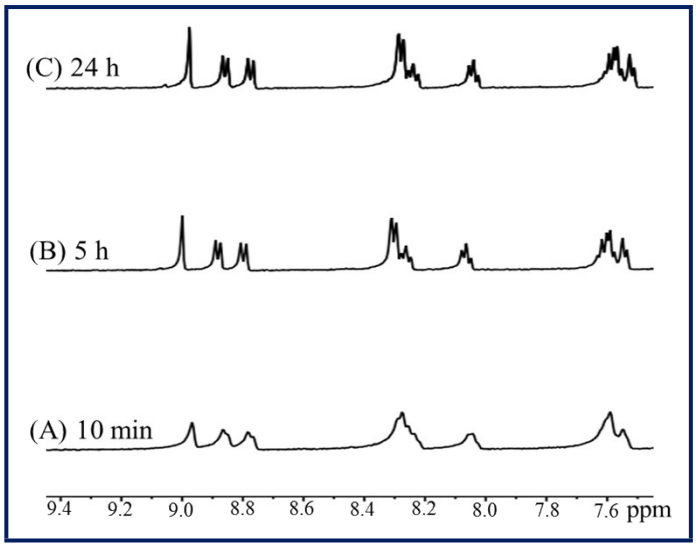

Figure S3. ^{1}H NMR spectra showing the hydrolysis of [(η^6-bz)Ru(L$_4$)Cl]PF$_6$ (**4**) (1 mM) in 50% MeOD-d_4/50% D_2O (v/v) at 310 K. (A) after 5 min; (B) after 5 h ; (C) after 24 h.

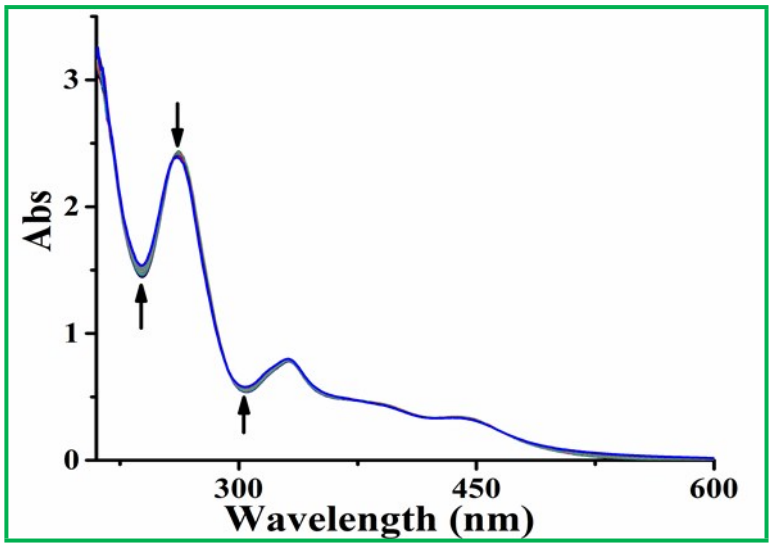

Figure S4. UV-Vis spectrum for a 50 μM solution of [(η^6-bz)Ru(L$_4$)Cl]PF$_6$ (**4**) in 30% MeOH/70% H_2O (v/v) recorded over a period of 8 h at 298 K.

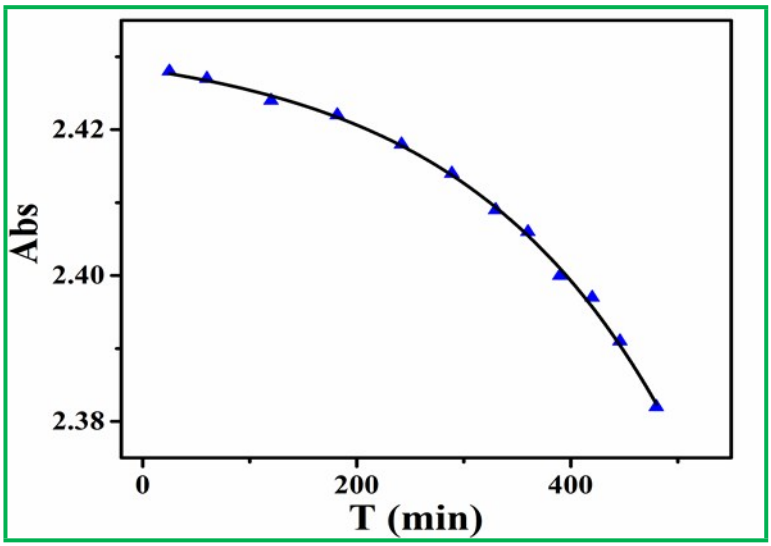

Figure S5. Time dependence of hydrolysis of **4** in 30% MeOH/70% H_2O (v/v) at 298 K based on UV-Vis spectrum by measuring the absorption difference.

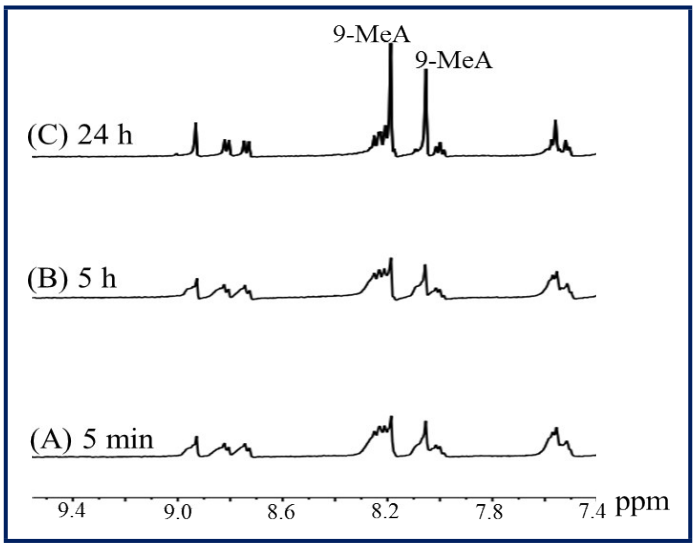

Figure S6. ^{1}H NMR spectra showing reaction of [(η^6-bz)Ru(L_4)Cl]PF_6 (**4**) with 9-methyladenine. (**A**) 5 min after the addition of 1 mol equiv 9-methyladenine to an equilibrium solution of complex 4 (1.0 mM) in 50% MeOD-d_4/50% D_2O (v/v) at 310 K; (**B**) after 5 h reaction; and (**C**) after 24 h. After 24 h, no reaction is observed.

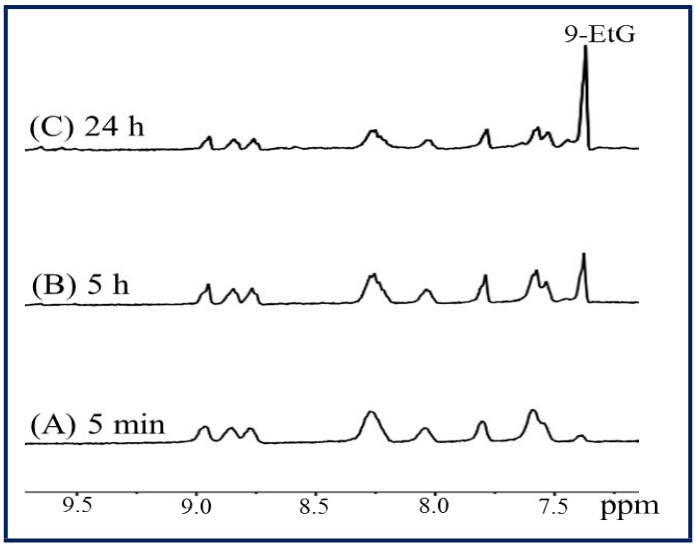

Figure S7. ^{1}H NMR spectra showing reaction of [(η^6-bz)Ru(L_4)Cl]PF_6 (**4**) with 9-ethylguanine. (**A**) 5 min after the addition of 1 mol equiv 9-ethylguanine to an equilibrium solution of complex **4** (1.0 mM) in 50% MeOD-d_4/50% D_2O (v/v) at 310 K; (**B**) after 5 h reaction; and (**C**) after 24 h. After 24 h, no reaction is observed.

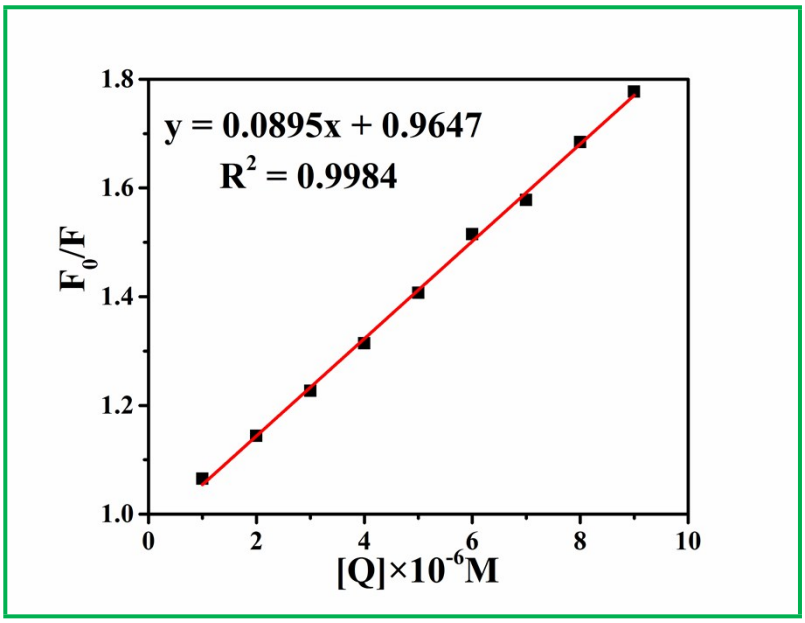

Figure S8. Stern-Volmer plots of F_0/F against the concentration of [(η^6-bz)Ru(L_4)Cl]PF_6 (**4**).

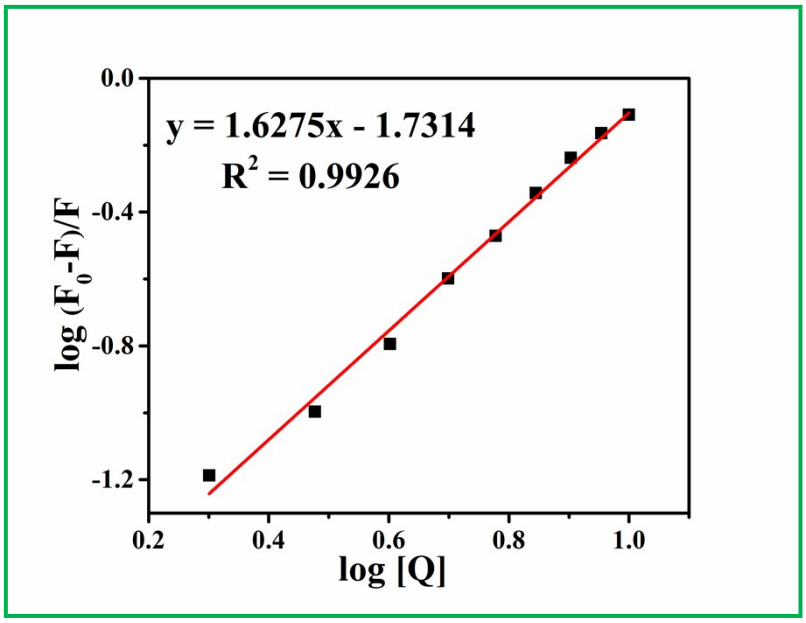

Figure S9. Plots of log [(F_0-F)/F] vs. log [Q] for the interaction of BSA with [(η^6-bz)Ru(L_4)Cl]PF_6 (**4**).

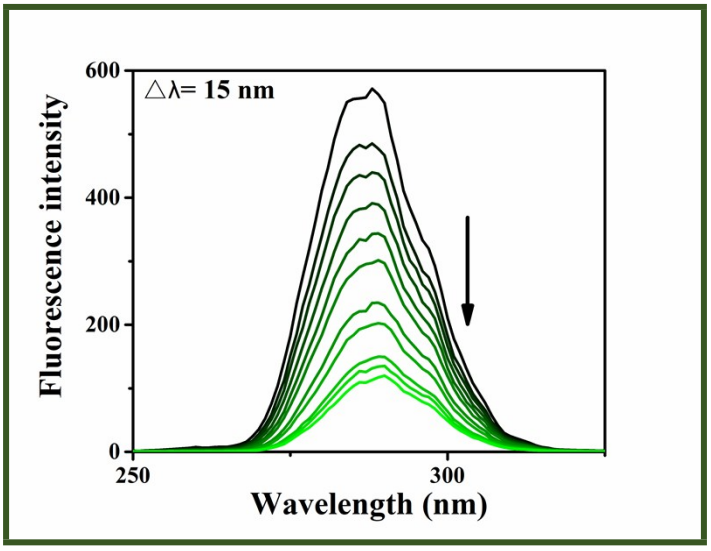

Figure S10. Synchronous spectra of BSA (20 μM) in the presence of increasing amounts of complex **4** (0-50 μM) with a wavelength Δλ = 15 nm.

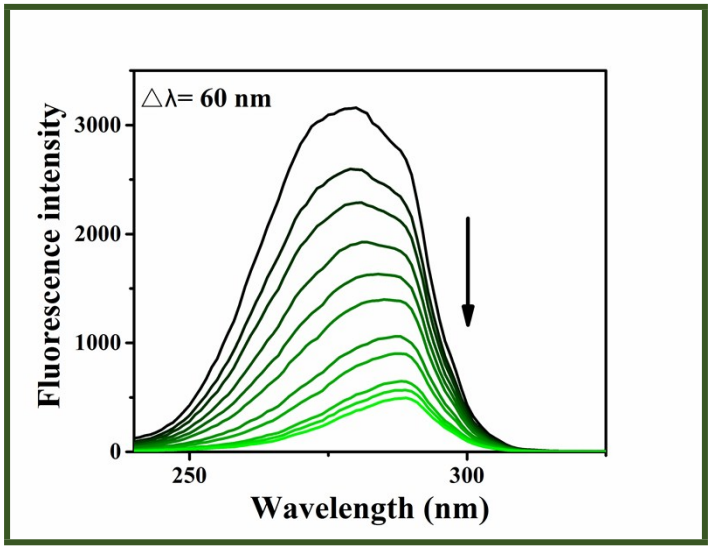

Figure S11. Synchronous spectra of BSA (20 μM) in the presence of increasing amounts of complex **4** (0-50 μM) with a wavelength Δλ = 60 nm.

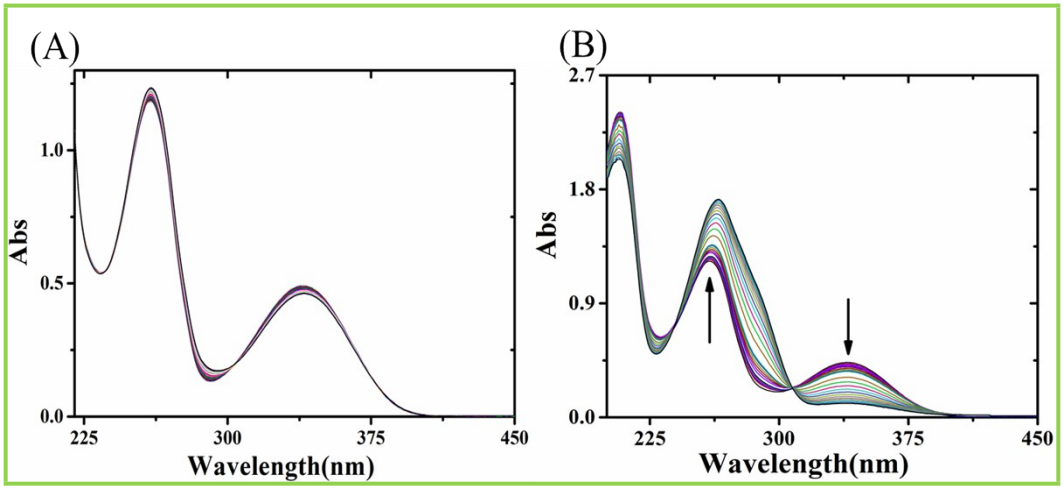

Figure S12. UV-Vis spectra of the reaction of NADH (100 μM) with complex **2** (1 μM) in 10% MeOH/90% H_2O (v/v) at 298 K for 8 h. (A) control: only NADH; (B) complex **2**.

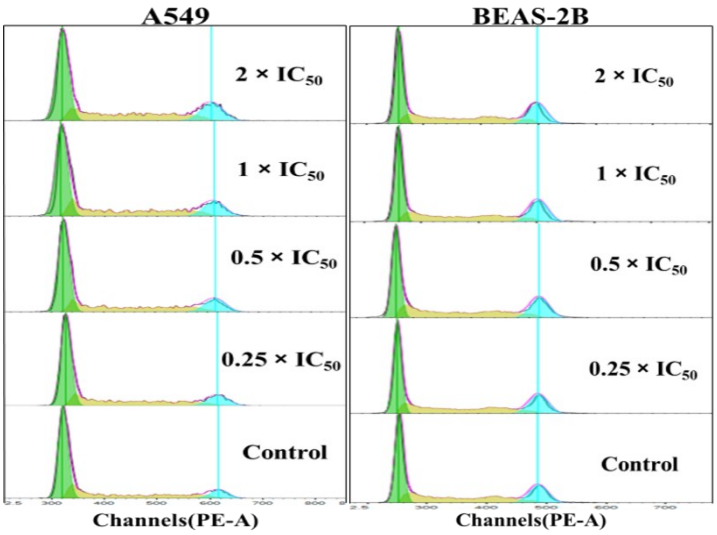

Figure S13. Flow cytometry data for cell cycle distribution of A549 cancer cells and BEAS-2B normal cells exposed to complex **4** for 24 h. Concentrations used were 0.25, 0.5, 1 and 2 equipotent concentrations of IC_{50}. Cell staining for flow cytometry was carried out using PI/RNase.

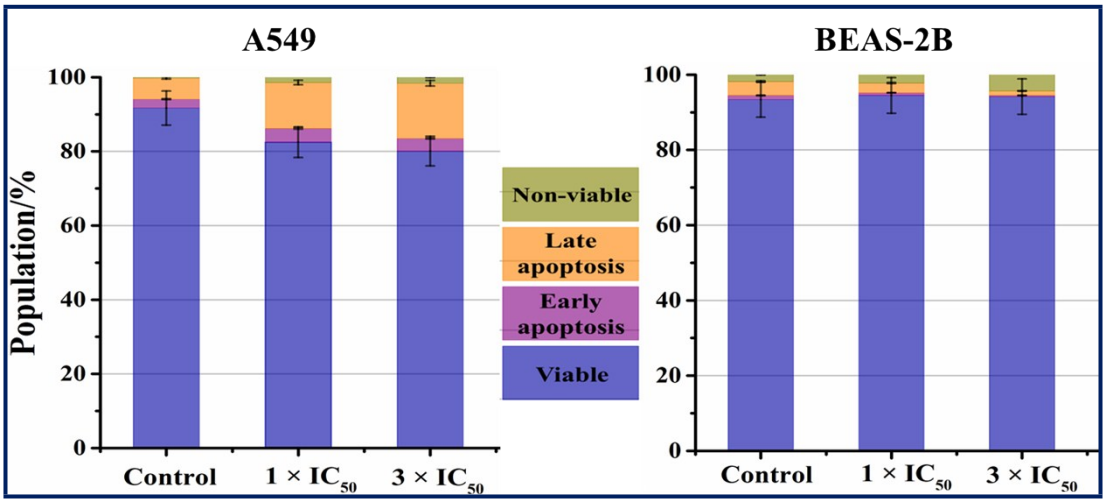

Figure S14. Apoptosis analysis of A549 and BEAS-2B cells after 24 h of exposure to complex **4** at 310 K determined by flow cytometry using annexin V-FITC vs PI staining. Populations for cells in four stages treated by complex **4**. Data are quoted as mean ± SD of three replicates.

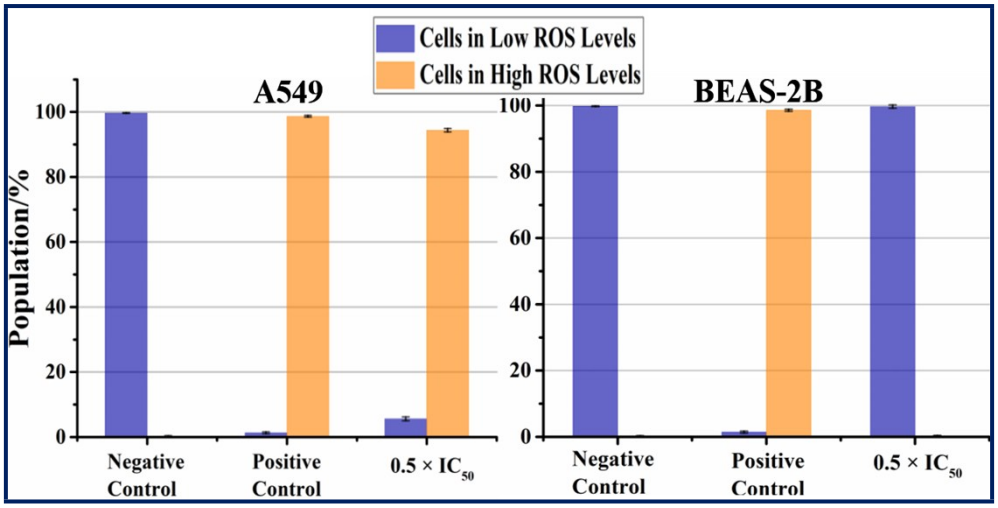

Figure S15. Flow cytometry analysis on ROS induction in A549 cancer cells and BEAS-2B normal cells treated with complex **4** at concentration of 0.5 × IC_{50}. Populations for cells in different ROS levels treated by complex **4**. Data are quoted as mean ± SD of three replicates.

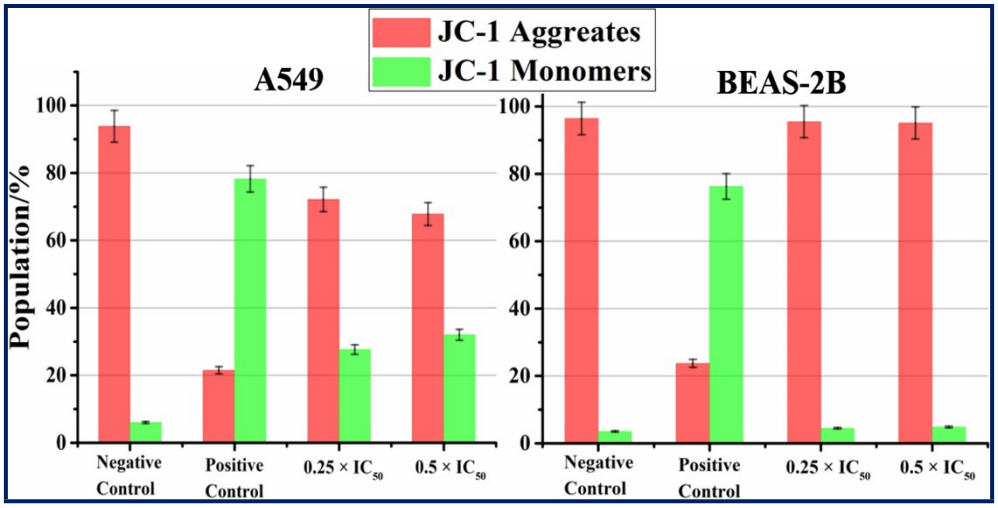

Figure S16. Changes in mitochondrial membrane potential of A549 cancer cells and BEAS-2B normal cells induced by complex **4** at concentrations of 0.25 × IC_{50} and 0.5 × IC_{50}. Populations of cells that exhibit a reduction in the mitochondrial membrane potential. Data are quoted as mean ± SD of three replicates.

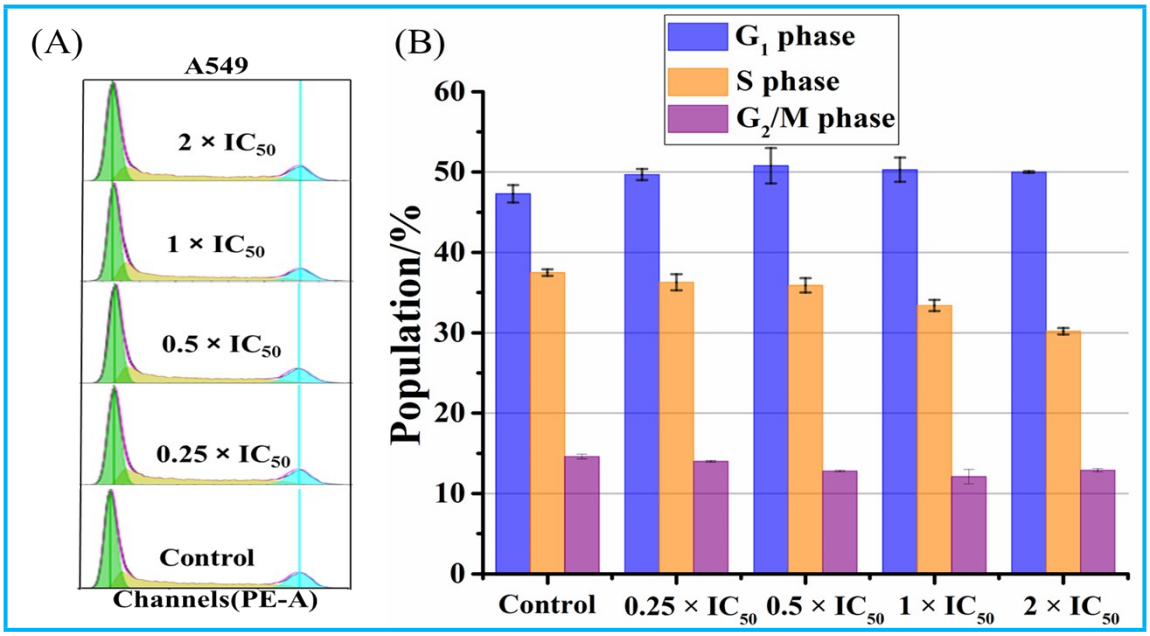

Figure S17. Flow cytometry data for cell cycle distribution of A549 cancer cells exposed to complex **2** for 24 h. Concentrations used were 0.25, 0.5, 1 and 2 equipotent concentrations of IC_{50}. Cell staining for flow cytometry was carried out using PI/RNase. (**A**) FL2 histogram for control (cells untreated) and complex **2** at various concentrations. (**B**) Cell populations in each cell cycle phase for control and complex **2**. Data are quoted as mean ± SD of three replicates.

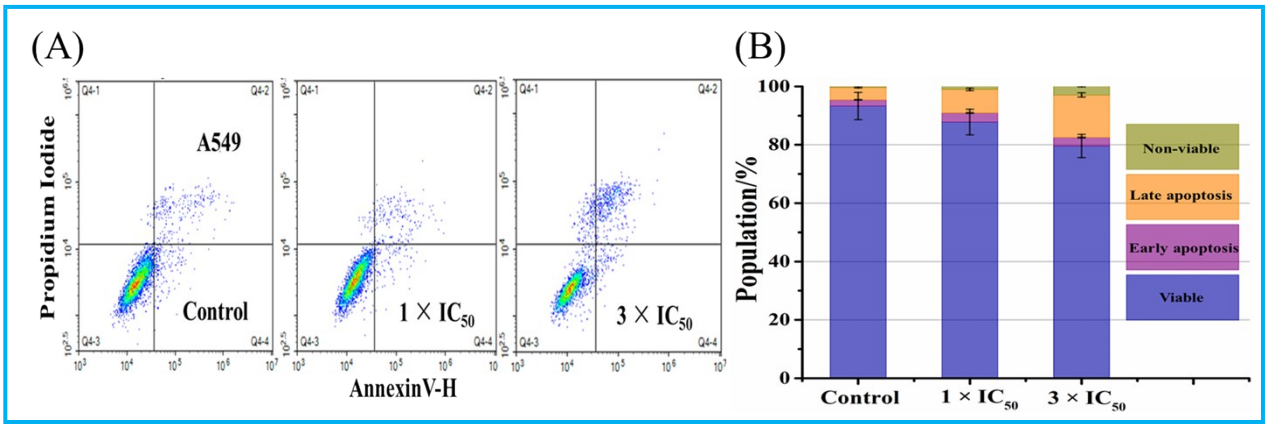

Figure S18. Apoptosis analysis of A549 cells after 24 h of exposure to complex **2** at 310 K determined by flow cytometry using annexin V-FITC vs PI staining. (**A**) Histogram for A549 cells treated with different concentrations of complex **2**; (**B**) Populations for cells in four stages treated by complex **2**. Data are quoted as mean ± SD of three replicates.

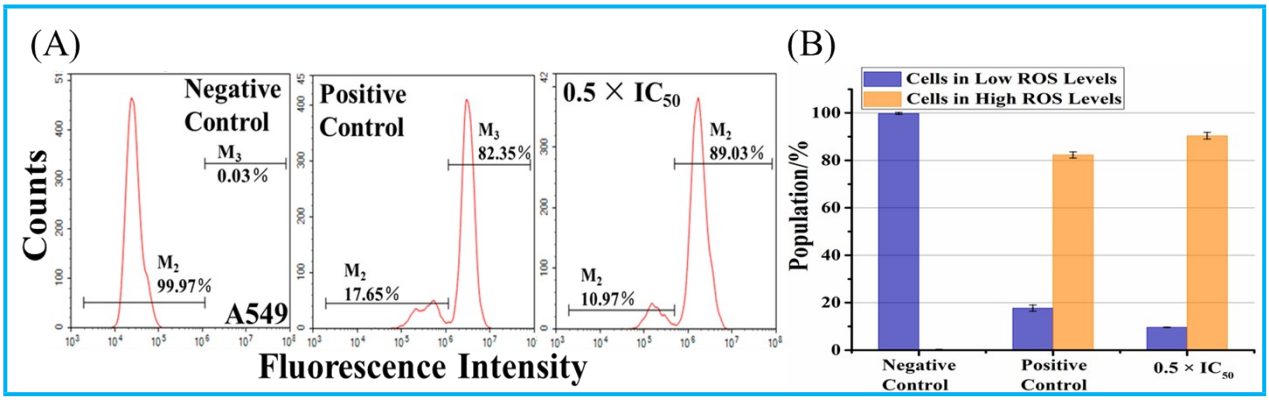

Figure S19. Flow cytometry analysis on ROS induction in A549 cancer cells treated with complex **2** at concentration of 0.5 × IC_{50}. (**A**) FL2 histogram for negative control (cells untreated), positive control and complex **2**. (**B**) Populations for cells in different ROS levels treated by **2**. Data are quoted as mean ± SD of three replicates.

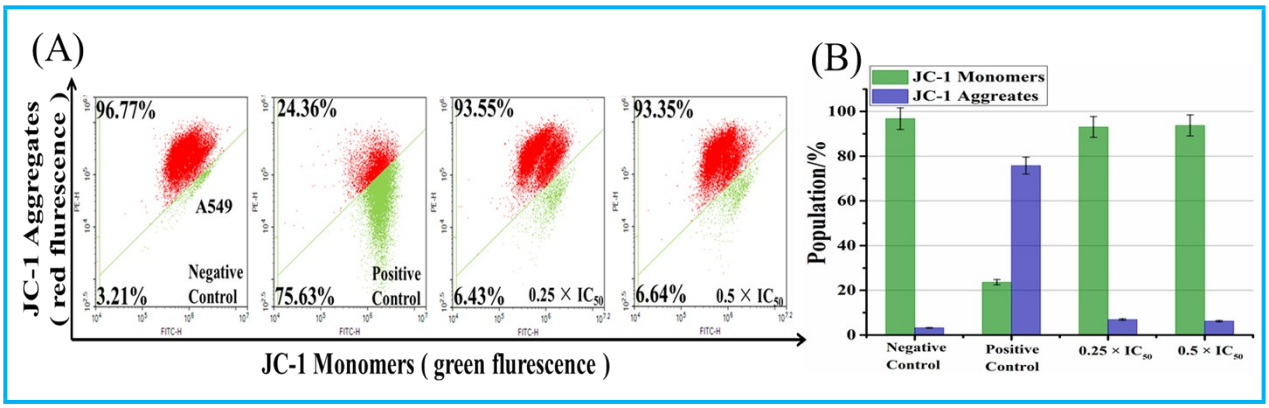

Figure S20. Changes in mitochondrial membrane potential of A549 cancer cells induced by complex **2**. (**A**) Flow cytometry histograms of the changes induced by the complex **2** at concentrations of 0.25 × IC_{50} and 0.5 × IC_{50}; (**B**) Populations of cells that exhibit a reduction in the mitochondrial membrane potential. Data are quoted as mean ± SD of three replicates.

Table S4. Cell cycle analysis carried out by flow cytometry using PI staining after exposing A549 cells to complex **4**.

		Population (%)		
Complex	**Ru concentration**	**G_1 phase**	**S phase**	**G_2/M phase**
4	0.25 × IC_{50}	56.9±0.3	32.1±1.3	12.2±0.3
	0.5 × IC_{50}	58.1±0.8	30.4±1.7	15.0±0.5
	1 × IC_{50}	55.5±0.6	33.3±2.8	16.4±0.4
	2 × IC_{50}	52.8±0.7	32.8±3.3	18.4±0.2
control		59.8±0.2	31.4±1.4	10.3±0.4

Table S5. Cell cycle analysis carried out by flow cytometry using PI staining after exposing BEAS-2B cells to complex **4**.

		Population (%)		
Complex	**Ru concentration**	**G_1 phase**	**S phase**	**G_2/M phase**
4	0.25 × IC_{50}	44.6±1.5	37.9±0.2	21.4±0.8
	0.5 × IC_{50}	47.5±1.3	36.8±0.6	23.4±0.9
	1 × IC_{50}	46.3±1.6	37.0±0.2	24.2±0.5
	2 × IC_{50}	44.0±0.8	38.5±0.9	24.5±2.5
control		47.8±0.5	37.3±0.2	21.8±1.0

Table S6. Flow cytometry analysis to determine the percentages of apoptotic cells, using Annexin V-FITC vs

PI staining, after exposing A549 ells to complex **4**.

Complex	Ru concentration	Population (%) Viable	Early apoptosis	Late apoptosis	Non-viable
4	$1 \times IC_{50}$	82.5±1.0	3.7±0.6	12.4±0.3	1.4±0.3
	$3 \times IC_{50}$	80.1±0.9	3.4±1.6	14.9±1.4	1.6±0.2
control		91.7±0.6	2.4±0.8	5.7±0.3	0.2±0.1

Table S7. Flow cytometry analysis to determine the percentages of apoptotic cells, using Annexin V-FITC vs PI staining, after exposing BEAS-2B cells to complex **4**.

Complex	Ru concentration	Population (%) Viable	Early apoptosis	Late apoptosis	Non-viable
4	$1 \times IC_{50}$	94.5±0.1	0.7±0.5	2.6±1.2	2.3±0.6
	$3 \times IC_{50}$	94.2±0.3	0.3±0.1	1.2±0.4	4.5±0.1
control		93.4±0.4	1.1±0.9	3.7±0.9	1.8±0.4

Table S8. ROS induction in A549 cancer cells treated with complex **4**.

Complex	Ru concentration	Population (%) Cells in low ROS levels	Cells in high ROS levels
4	0.5 × IC_{50}	5.6±0.6	94.4±0.6
Untreated cells (Negative Control)		99.7±0.1	0.3±0.1
CCCP treated cells (Positive Control)		1.3±0.3	98.7±0.3

Table S9. ROS induction in BEAS-2B normal cells treated with complex **4**.

Complex	Ru concentration	Population (%) Cells in low ROS levels	Cells in high ROS levels
4	0.5 × IC_{50}	99.7±0.5	0.3±0.1
Untreated cells (Negative Control)		99.8±0.7	0.2±0.1
CCCP treated cells (Positive Control)		1.4±0.3	98.6±0.3

Table S10. The mitochondrial membrane polarization of A549 cells induced by complex **4**.

Complex	Ru concentration	Population (%) JC-1 Aggregates	JC-1 Monomers
4	0.25 × IC_{50}	71.1±0.2	27.1±0.6
	0.5 × IC_{50}	67.0±0.7	31.7±0.4
Negative Control		93.7±0.2	6.5±0.4
Positive Control		21.4±0.6	78.2±0.5

Table S11. The mitochondrial membrane polarization of BEAS-2B cells induced by complex **4**.

Complex	Ru concentration	Population (%) JC-1 Aggregates	JC-1 Monomers
4	0.25 × IC_{50}	95.8±0.3	4.2±0.3
	0.5 × IC_{50}	95.2±0.4	4.5±0.6
Negative Control		95.9±0.6	3.8±0.2
Positive Control		22.6±1.2	75.7±0.5

Table S12. Cell cycle analysis carried out by flow cytometry using PI staining after exposing A549 cells to complex **2**.

Complex	Ru concentration	Population (%)		
		G_1 phase	S phase	G_2/M phase
2	0.25 × IC_{50}	49.7±0.7	36.3±1.0	14.0±0.1
	0.5 × IC_{50}	51.8±2.2	35.9±0.9	12.8±0.1
	1 × IC_{50}	50.3±1.5	33.4±0.7	12.1±0.9
	2 × IC_{50}	50.0±0.1	30.2±0.4	12.9±0.2
control		47.3±1.1	37.5±0.4	14.6±0.3

Table S13. Flow cytometry analysis to determine the percentages of apoptotic cells, using Annexin V-FITC vs PI staining, after exposing A549 ells to complex **2**.

Complex	Ru concentration	Population (%)			
		Viable	Early apoptosis	Late apoptosis	Non-viable
2	1 × IC_{50}	87.8±0.2	3.1±0.1	8.1±0.4	1.1±0.2
	3 × IC_{50}	79.6±1.0	2.9±0.6	14.6±1.0	2.9±1.4
control		93.3±0.1	2.1±0.9	4.3±0.9	0.4±0.1

Table S14. ROS induction in A549 cancer cells treated with complex **2**.

Complex	Ru concentration	Population (%)	
		Cells in low ROS levels	Cells in high ROS levels
2	$0.5 \times IC_{50}$	9.6±0.4	90.4±1.4
Untreated cells (Negative Control)		99.8±0.2	0.2±0.1
CCCP treated cells (Positive Control)		17.7±1.3	82.3±1.3

Table S15. The mitochondrial membrane polarization of A549 cancer cells induced by complex **2**.

Complex	Ru concentration	Population (%)	
		JC-1 Aggregates	JC-1 Monomers
2	$0.25 \times IC_{50}$	93.1±0.7	6.9±0.7
	$0.5 \times IC_{50}$	93.8±0.6	6.2±0.6
Negative Control		96.8±0.3	3.2±0.3
Positive Control		23.6±0.9	75.8±0.4

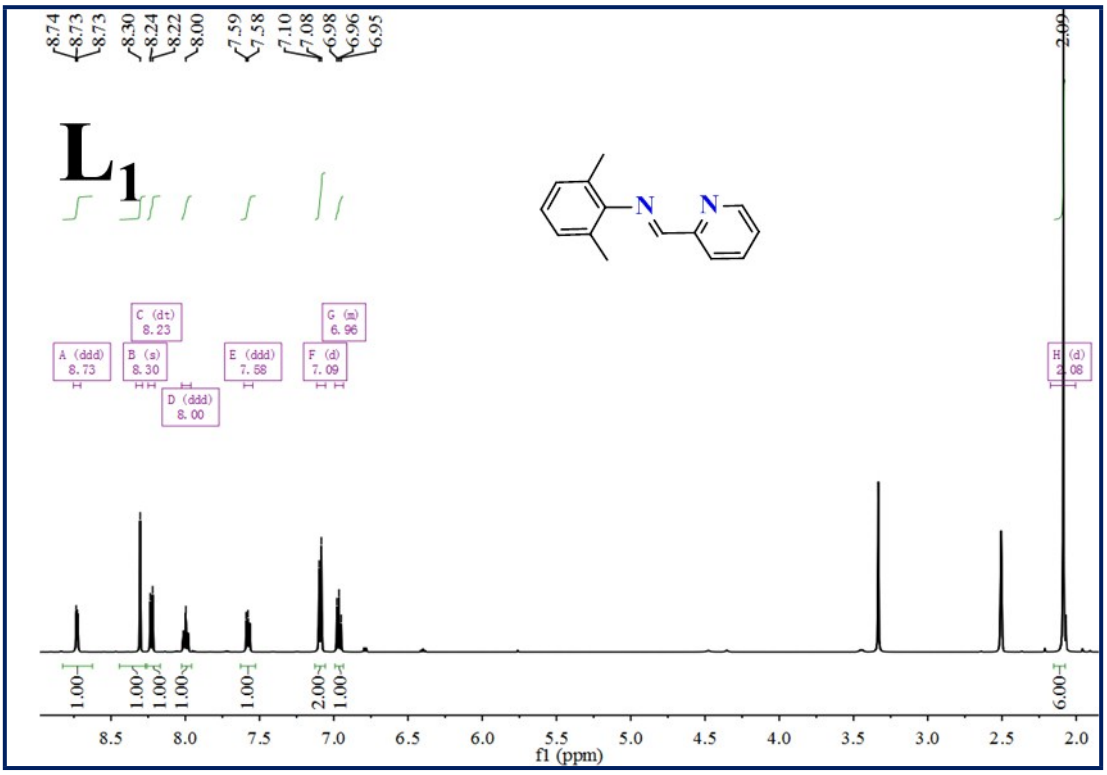

Figure S21. The ^{1}H NMR (500.13 MHz, DMSO) peak integrals of $\mathbf{L_1}$.

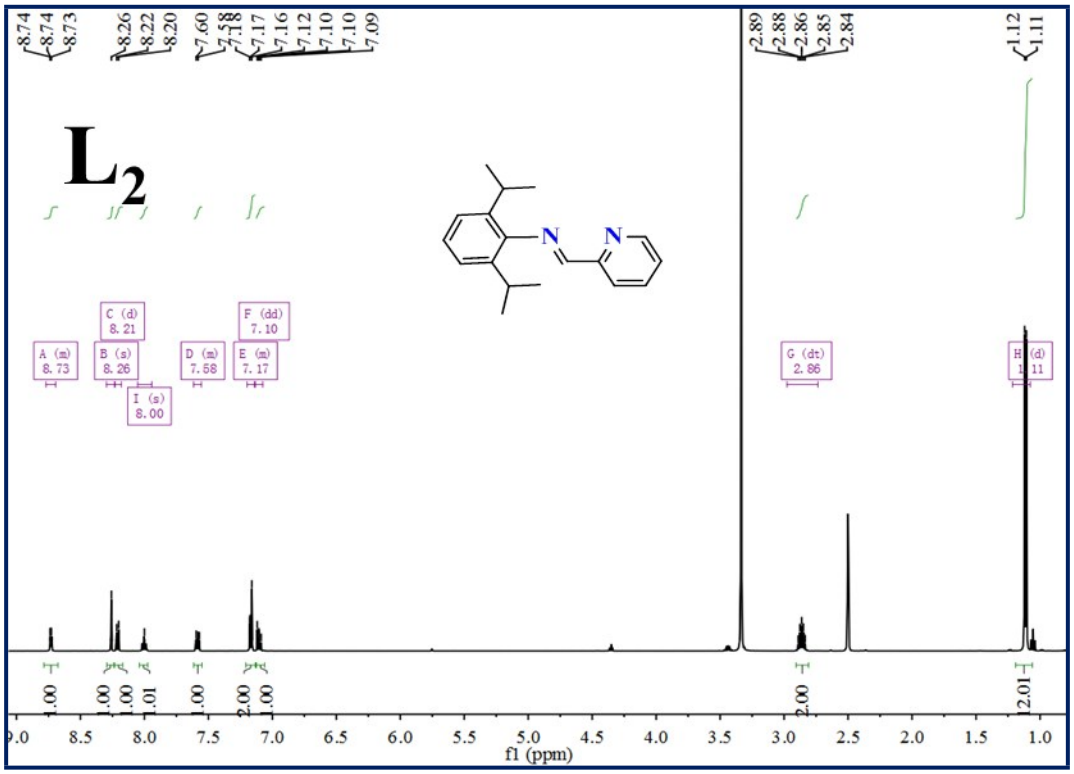

Figure S22. The ^{1}H NMR (500.13 MHz, DMSO) peak integrals of $\mathbf{L_2}$.

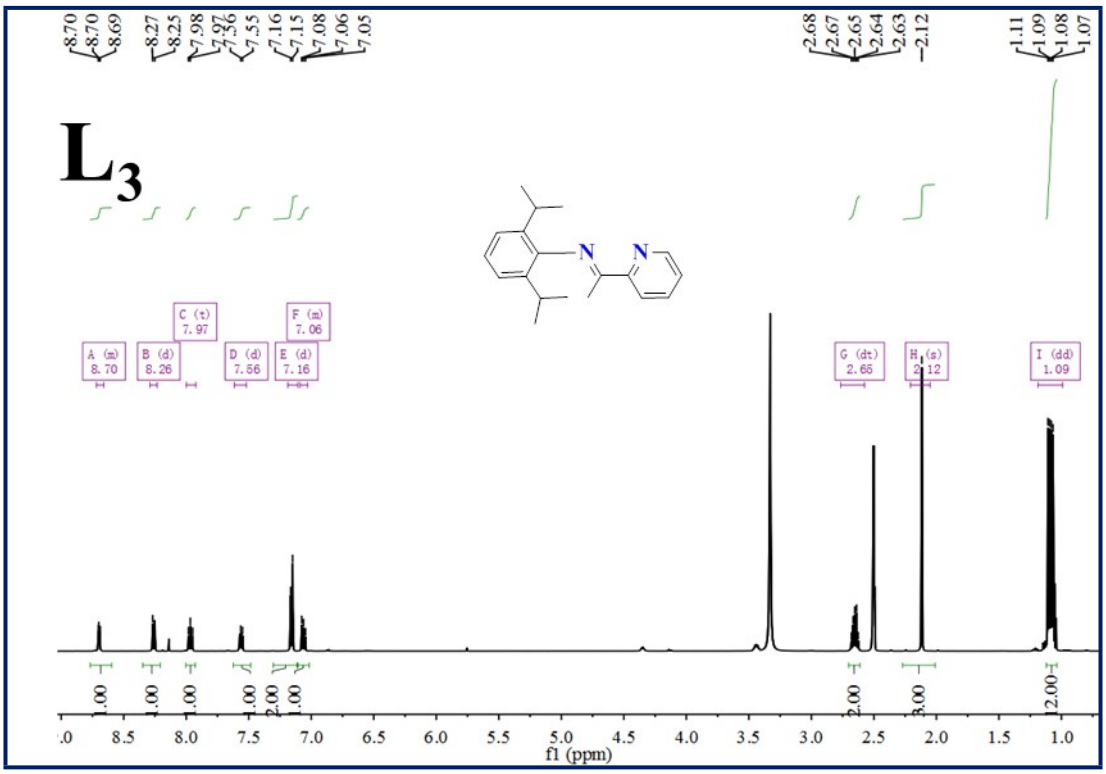

Figure S23. The ^{1}H NMR (500.13 MHz, DMSO) peak integrals of $\mathbf{L_3}$.

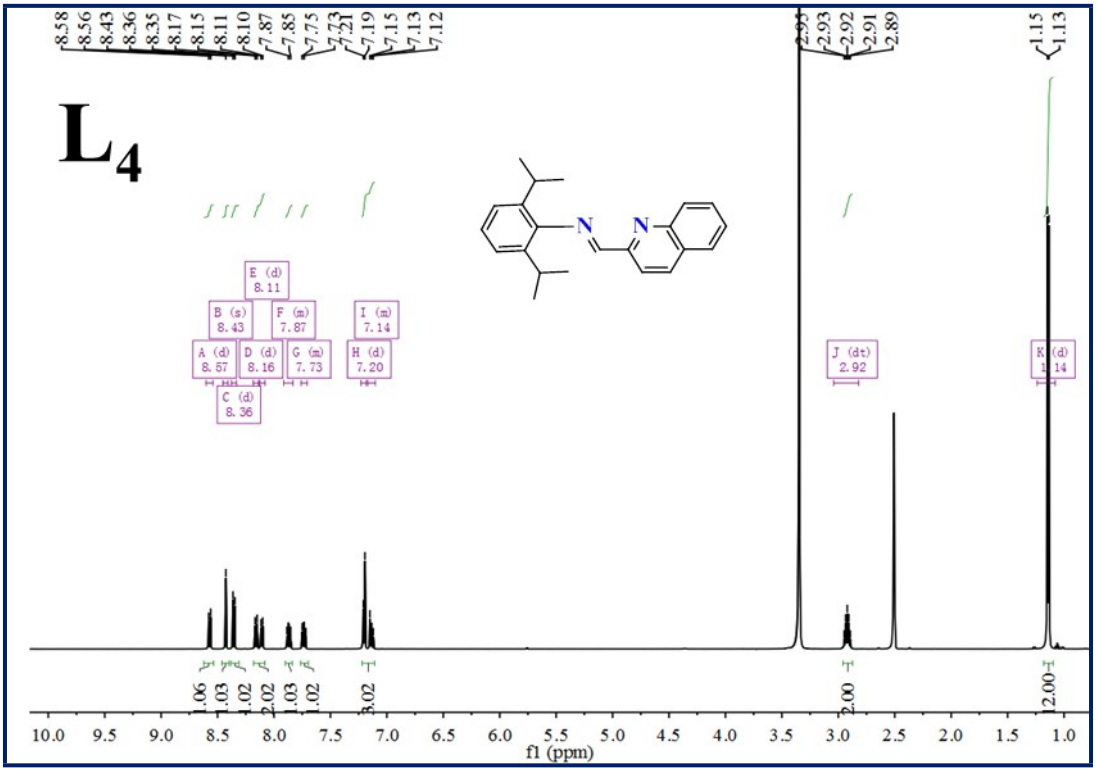

Figure S24. The ^{1}H NMR (500.13 MHz, DMSO) peak integrals of $\mathbf{L_4}$.

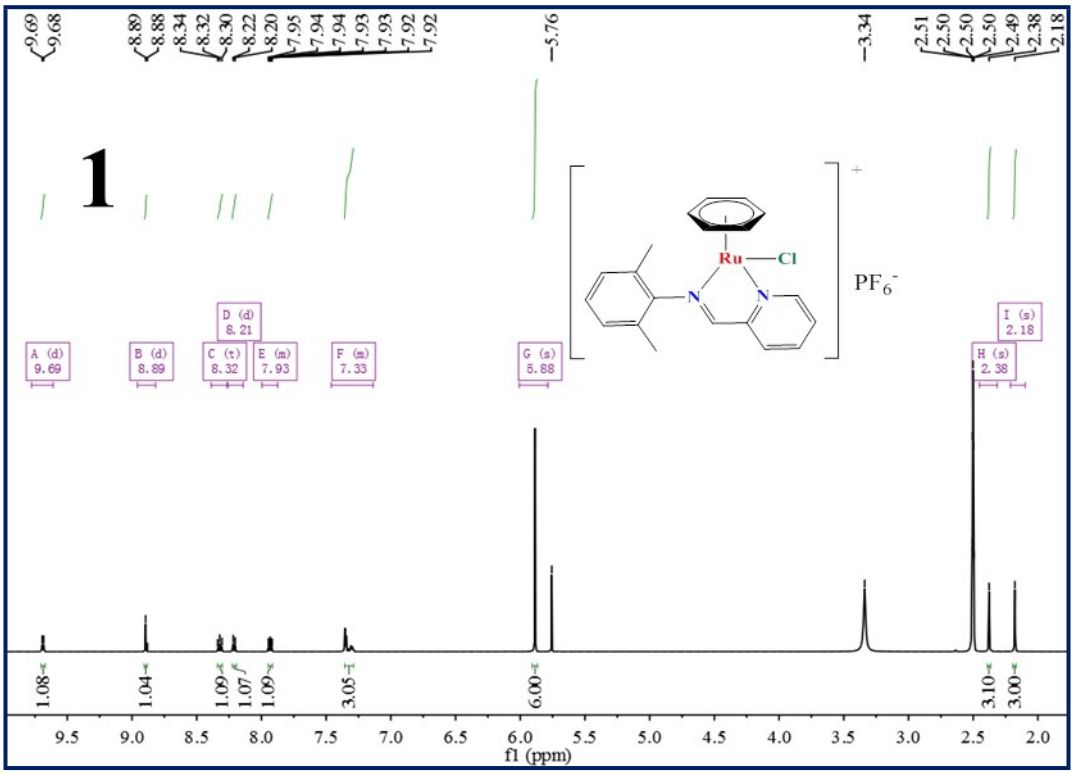

Figure S25. The ^{1}H NMR (500.13 MHz, DMSO) peak integrals of [(η^6-bz)Ru(L_1)Cl]PF_6 (**1**).

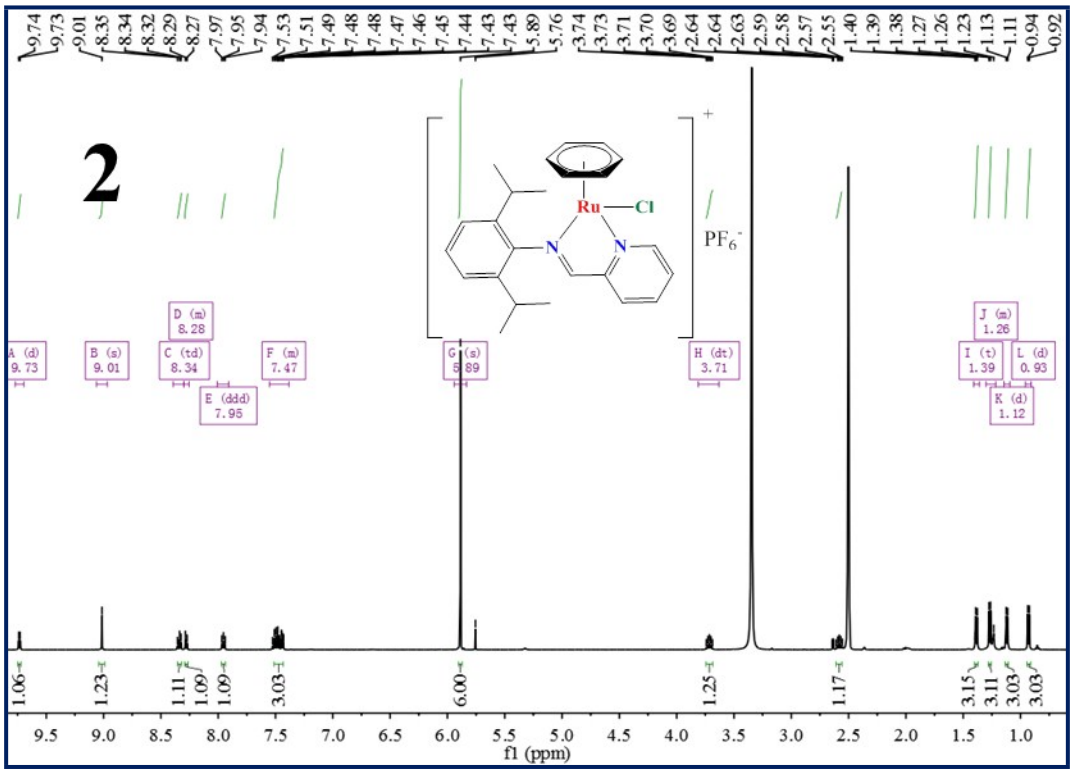

Figure S26. The ^{1}H NMR (500.13 MHz, DMSO) peak integrals of [(η^6-bz)Ru(L_2)Cl]PF_6 (**2**) .

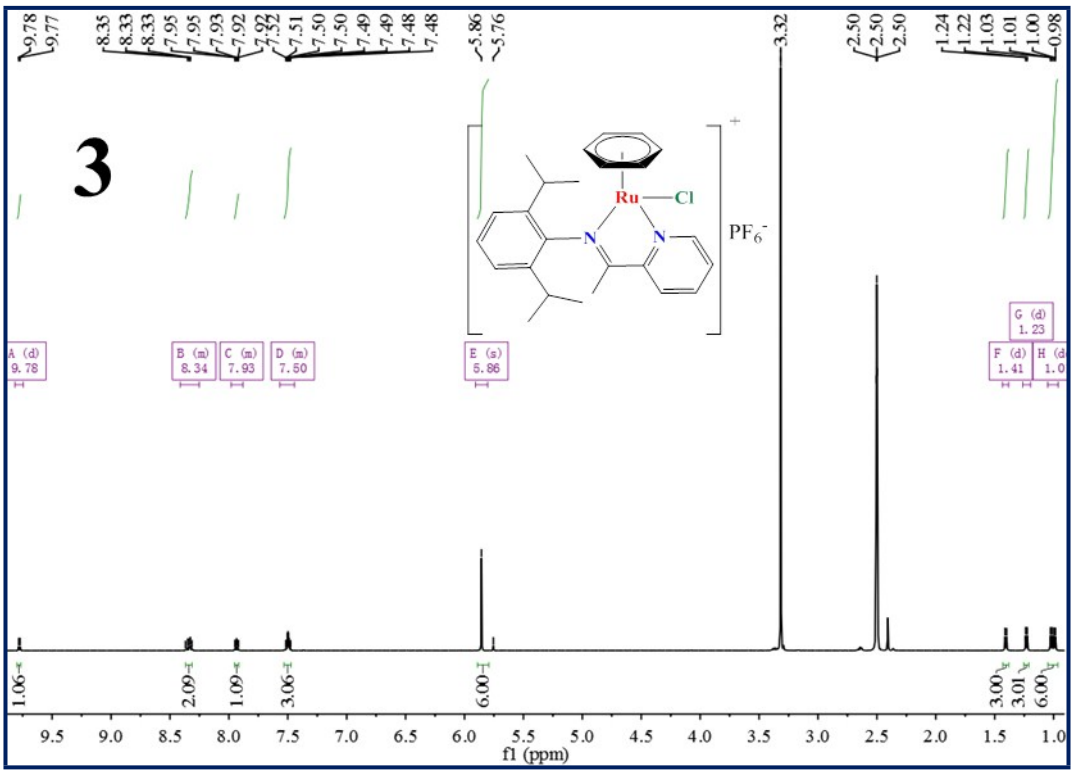

Figure S27. The ^{1}H NMR (500.13 MHz, DMSO) peak integrals of [(η^6-bz)Ru(L_3)Cl]PF_6 (**3**) .

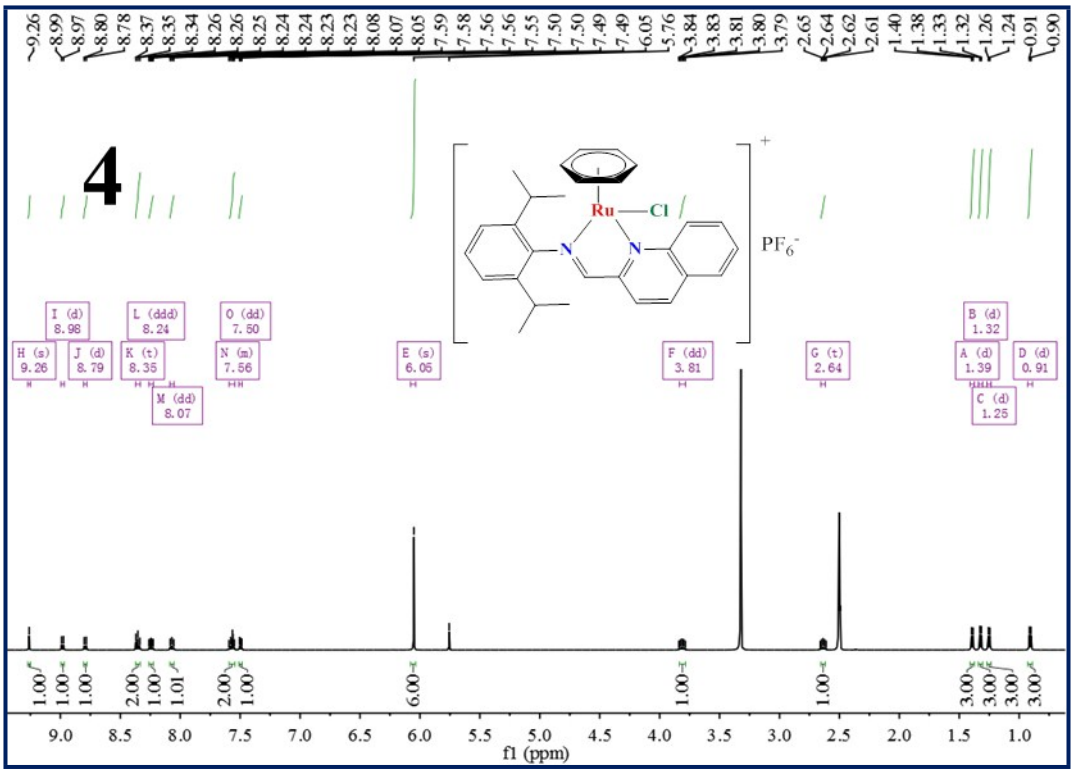

Figure S28. The ^{1}H NMR (500.13 MHz, DMSO) peak integrals of [(η^6-bz)Ru(L_4)Cl]PF_6 (**4**) .

[(η^6-bz)Ru(L_1)Cl]PF_6 (**1**)

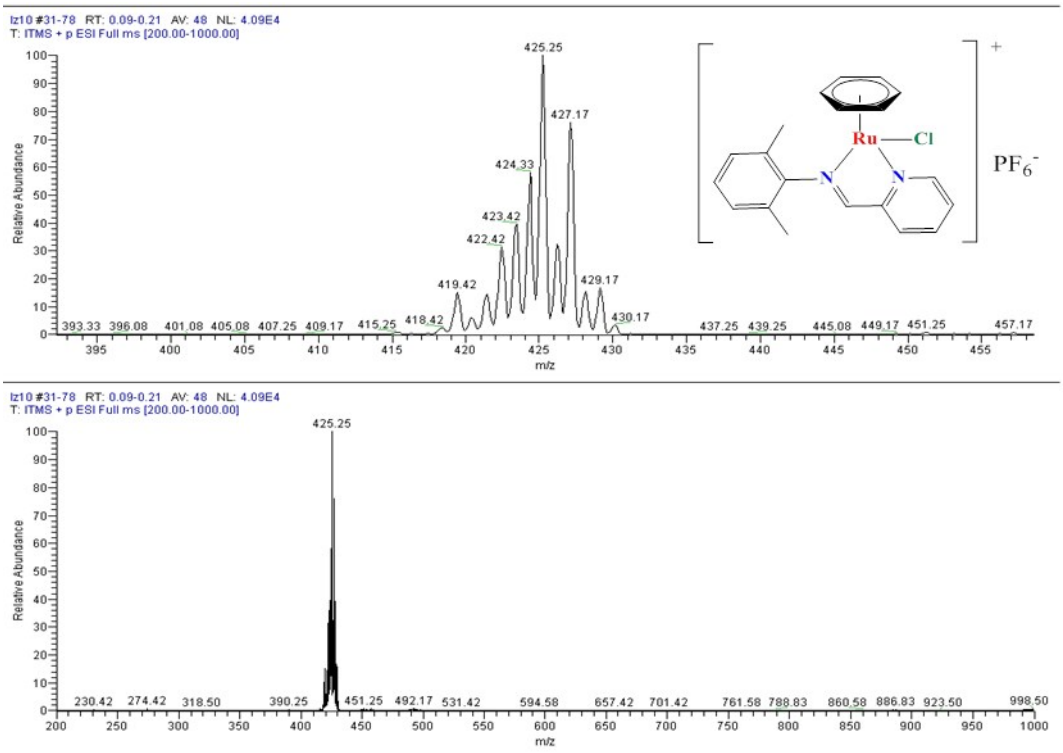

[(η^6-bz)Ru(L_2)Cl]PF_6 (**2**)

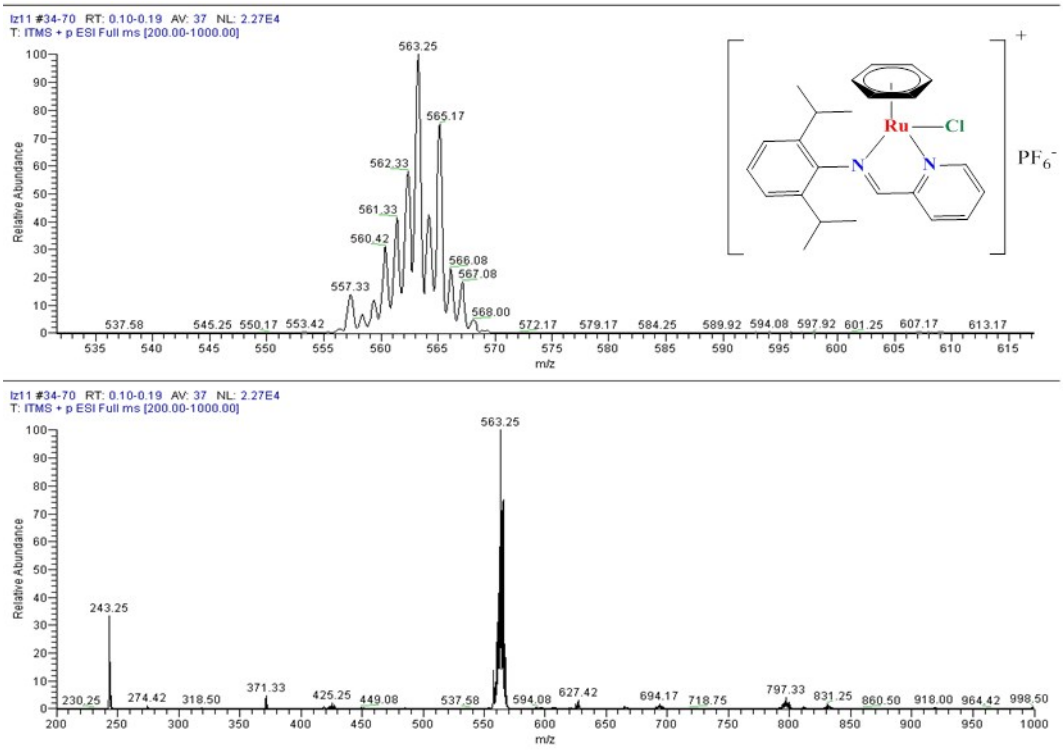

[(η^6-bz)Ru(L_3)Cl]PF_6 (**3**)

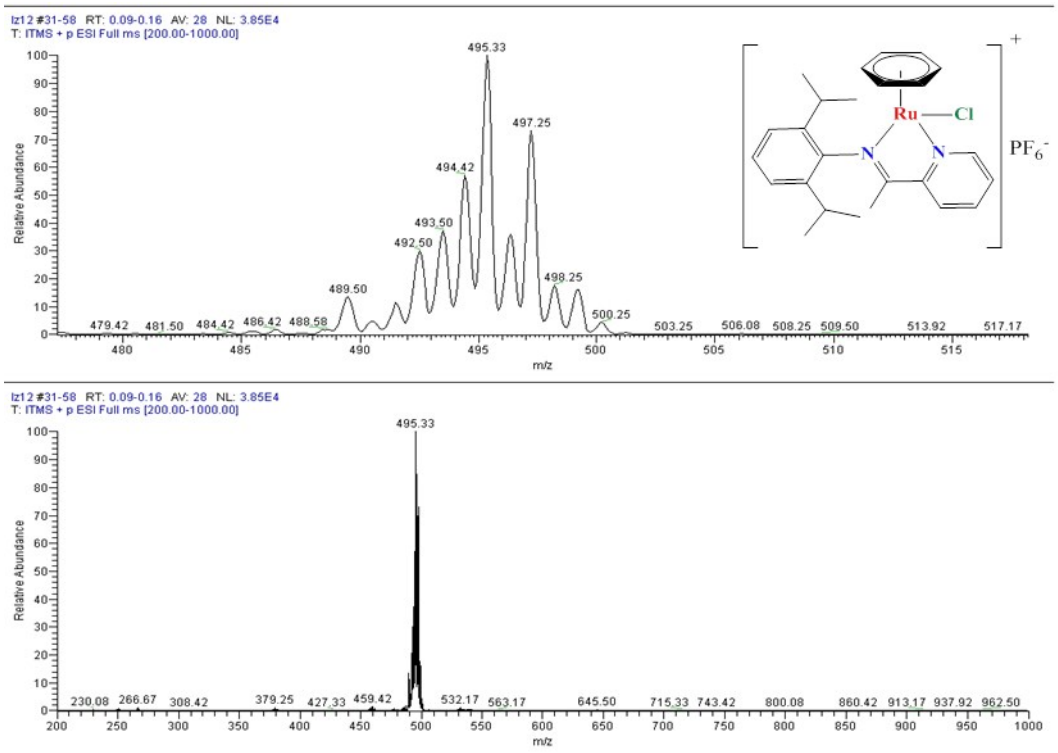

[(η^6-bz)Ru(L_4)Cl]PF_6 (**4**)

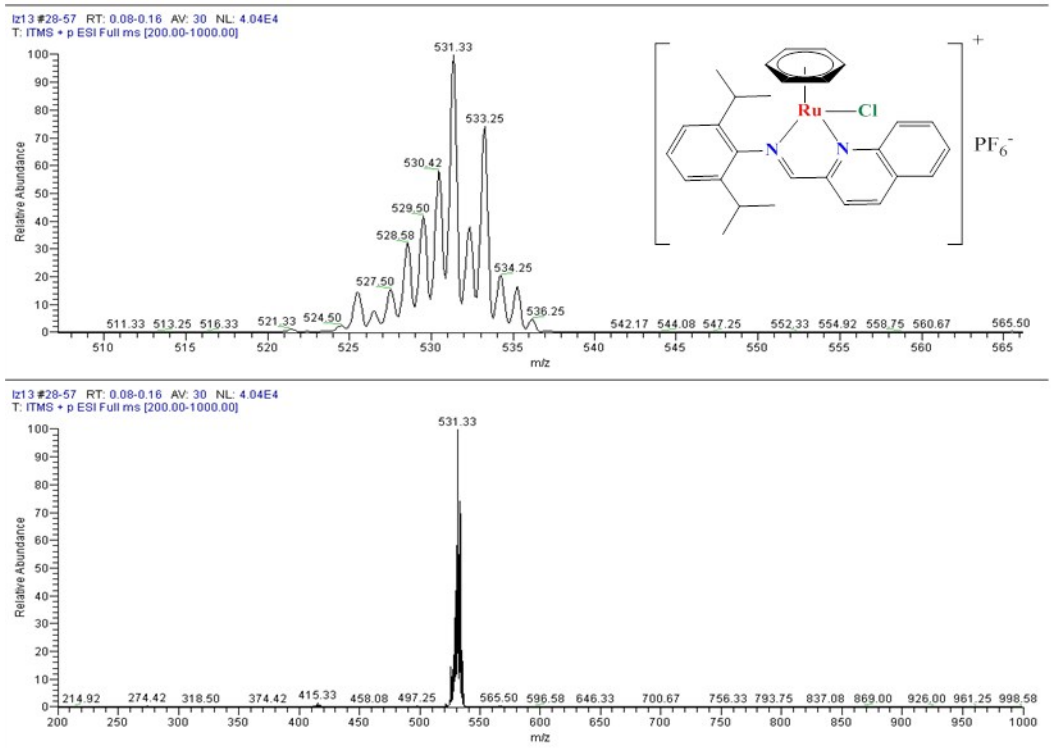

Figure S29. The Mass spectrometry of complexes **1**-**4** [(η^6-bz) Ru(N^N)Cl]PF_6 .